Int J Adv Manuf Technol (2017) 91:1879–1887
DOI 10.1007/s00170-016-9944-y

ORIGINAL ARTICLE

Resistance spot welding quality identification with particle swarm optimization and a kernel extreme learning machine model

Hongchun Sun[1] · **Jianhui Yang**[1] · **Lina Wang**[1]

Received: 13 July 2016 / Accepted: 18 December 2016 / Published online: 28 December 2016
© Springer-Verlag London 2016

Abstract To target the accurate and fast joint quality identification, this work presents a method based on the particle swarm optimization (PSO) and the kernel extreme learning machine (KELM) in resistance spot welding (RSW). We perform welding and tensile tests to determine the related information and extract features from signals combined with the welding mechanism. Afterward, we optimize the parameters in the KELM with the PSO and fivefold cross validation (CV) and establish an identification model based on the KELM to classify the joint quality. The comparison results show that the joint quality identification model has a good generalization performance with an accuracy of up to 97.83%. Moreover, the feature extraction is reasonable, providing insight into the RSW process. The quality identification method based on the PSO and KELM is effective in RSW.

Keywords Resistance spot welding · Particle swarm optimization · Kernel extreme learning machine · Pattern recognition · Joint quality

✉ Hongchun Sun
hchsun@mail.neu.edu.cn

Jianhui Yang
yjh_neu@163.com

Lina Wang
lnw_neu@163.com

[1] School of Mechanical Engineering and Automation, Northeastern University, Shenyang 110819, China

1 Introduction

With its higher cost performance, resistance spot welding (RSW) is widely used in industrial fields. The related product reliability depends, in part, on the joint quality. However, the traditional joint quality test is destructive, sampling and offline [1], which neither guarantees the accuracy and real-time detection nor meets the cost control principles. Therefore, considerable research on joint quality has been conducted by scholars, which has led to numerous joint quality analysis methods. Generally, these methods can be divided into the following two categories: statistical analysis methods [2–5] and artificial intelligence methods [6–9]. To predict the joint quality, Luo Y et al. [2] used regression analysis to build a nonlinear multiple regression to forecast a model between the welding features and the joint quality indexes (shear strength and nugget diameter). Due to the high nonlinearity and multivariable coupling in the RSW process, scholars turn their attention to the neural network to solve highly nonlinear and uncertain problems. Wan X et al. [6] designed a BP neural network, which predicts the weld nugget size and the fatigue load value. Even though the artificial neural network is widely used in spot welding quality identification, there are still some unavoidable deficiencies, such as the excessive reliance on training samples and the ease of being trapped in a local minimum. In recent years, novel methods using intuitive images to present joint quality have been proposed [10, 11]. Study [10] used the Chernoff faces technique to present the joint quality.

Although different methods are adopted in the above studies, these works can effectively classify the RSW quality. However, there are some aspects that need further consideration. For instance, obtaining a higher RSW quality identification requires complex and labour-intensive work, such as developing the network structure and the variables to describe

the intuitive chart. It has been suggested that the support vector machine (SVM) and the extreme learning machine (ELM) have improved generalization performance, fast training speed, and easy implementation. Compared with SVM, the ELM can achieve better generalization performance at a faster speed for multiclassification [12, 13]. In addition, there is little research related to RSW quality identification based on ELM. Therefore, this study considers the ease of implementation and improved generalization performance for RSW quality identification. We propose a joint quality identification method using the particle swarm optimization (PSO) and kernel extreme learning machine (KELM). The results strengthen our comprehension of the RSW process and the method based on PSO and KELM can be a supplement to the joint quality identification.

The outline of this paper is as follows. The concepts of PSO and KELM are briefly reviewed in "Section 2", "Section 3" presents the RSW data acquisition, "Section 4" provides the feature extraction in the RSW, and "Section 5" classifies the RSW quality. Finally, "Section 6" concludes the study.

2 Review of PSO and KELM

2.1 PSO

Particle swarm optimization, proposed by Kennedy and Eberhart [14] in 1995, is a swarm intelligence optimization algorithm in the field of computational intelligence and is used to solve optimization problems. In the algorithm, each particle represents a potential solution to the optimization problem and corresponds to a value that is determined by the fitness function. Each particle's velocity determines the moving direction and distance in accordance with its and other particles' motion to finish the dynamic adjustment. Then, the optimization in the solution space is achieved [15].

At each iteration, the particles update their velocity and position by comparing the fitness value, personal optimal solution, and the global optimal solution.

$$V_{id}^{k+1} = \omega V_{id}^{k} + c_1 r_1 \left(P_{id}^{k} - X_{id}^{k}\right) + c_2 r_2 \left(P_{gd}^{k} - X_{id}^{k}\right) \quad (1)$$

$$X_{id}^{k+1} = X_{id}^{k} + V_{id}^{k+1} \quad (2)$$

where ω is the inertial weight that determines the extent of the previous particle's velocity affecting the current and plays a role in balancing the global and local search. k is the current number of iterations. V_{id} and X_{id} are the particle's velocity and position, respectively, c_1 and c_2 are learning factors, and r_1 and r_2 are random numbers in [0, 1]. To avoid blind searching, we limit the velocity and position of these particles to the ranges $[-V_{\max}, V_{\max}]$ and $[-X_{\max}, X_{\max}]$.

The PSO algorithm has a fast convergence speed, good robustness, and strong commonality. In this paper, we use the PSO to optimize the penalty parameter, C, and kernel parameter, g, in the KELM. We set the iteration number to 100, and the size of the population is set to 20 in the PSO. Meanwhile, to avoid the problems of premature convergence and low iteration efficiency in later periods, we introduce the mutation into the PSO algorithm, which can expand the search space to ensure population diversity and improve the ability to search the optimal solution.

2.2 KELM

The extreme learning machine is a new algorithm of the single-hidden-layer feed-forward neural network (SFLN). The hidden layer offset and connection weights between an input layer and a hidden layer, which remain constant in the training process, are randomly generated by the algorithm. The sole interaction is setting the number of hidden layer neurons. Afterward, the optimal solution is obtained [16, 17].

Given a training data set, $x_i \in R^n$, $t_i \in R^q$, and $i = 1, \ldots, N$, a standard SFLN with L nodes in the hidden layer and the activation function $f(x)$ provides the following mathematical model.

$$\sum_{i=1}^{L} \beta_i f\left(\omega_i \cdot x_j + b_i\right) = O_j \qquad j = 1, ..., N \quad (3)$$

where ω_i is the input weight between the ith input neuron and the hidden layer node. b_j is the bias of the ith hidden layer node, β_i is the output weight vector connecting the hidden layer and output layer, and O_j is the output value of the j th input sample.

Huang et al. proposed and proved that when the hidden layer nodes and sample number are consistent, there is zero error in approximating N samples for any input weight and bias.

$$\sum_{i=1}^{L} \beta_i f\left(\omega_i \cdot x_j + b_i\right) = t_j, \quad j = 1, ..., N \quad (4)$$

where t_j is the real value of the jth sample. Eq. (4) can be rewritten as Eq. (5).

$$H\beta = T \quad (5)$$

where H is the hidden layer output matrix. The output weight, β, can be achieved through the least-square solutions.

$$\beta = H^{+}T \quad (6)$$

where H^{+} is Moore-Penrose of H.

To improve the robustness and generalization performance of the ELM, Huang et al. introduced the kernel matrix, defined by Eq. (7) in the ELM, and the proposed kernel extreme learning machine.

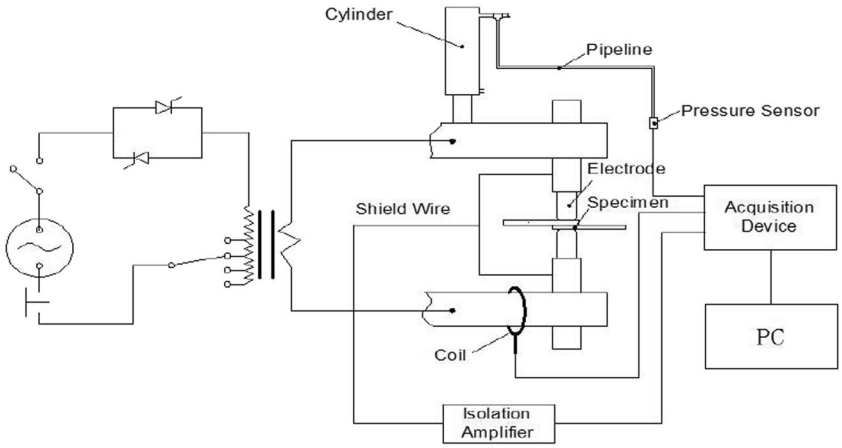

Fig. 1 Layout diagram of the testing system

$$\Omega_{\mathrm{KELM}} = HH^T \qquad \Omega_{i,j} = h(x_i)h(x_j) = K(x_i,x_j) \tag{7}$$

The output of the KELM is,

$$f(x) = h(x)\beta = h(x)H^T\left(HH^T + \frac{I}{C}\right)^{-1}T = \begin{bmatrix} K(x,x_1) \\ \vdots \\ K(x,x_N) \end{bmatrix}^T \left(\frac{I}{C} + \Omega_{\mathrm{KELM}}\right)^{-1}T \tag{8}$$

where $K(x,x_j)$ is the kernel function, C is the penalty parameter that balances the empirical risk and structural risk, I is the identity matrix, and Ω_{KELM} is the kernel matrix. In this paper, the RBF kernel, $K(u,v) = -\|u-v\|^2/g$, is adopted. The penalty parameter, C, and kernel parameter, g, in the KELM play crucially important roles in model construction.

3 Spot welding data acquisition

3.1 Signal test system

Figure 1 shows the signal test system. In the spot welding process, the acquisition system collects the following three signals: current, voltage, and electrode pressure. The current signal is transmitted to the acquisition system by a Rogowski coil (CY-RCTA02-Φ120, UK). The voltage signal can be directly obtained from the electrode, passing by the shielded wire and isolation module (ISO-U1-P3-O4, People's Republic of China.). The electrode pressure signal is the output pressure of the cylinder converted by the pressure sensor (MPX5700AP, USA). After a series of filtering and denoising processes, three signals are displayed and stored in the PC.

Table 1 RWMA recommended welding parameters

Welding time (*t*/Cycle)	Welding current (*I*/A)	Welding pressure (*F*/N)
8	8800	2250

3.2 Spot welding test

A DNT3-200 (spot-welding machine, People's Republic of China) adopts the constant-current control pattern. The specimen used is the Q235, whose size is 100 × 20 × 1.0 mm, and the overlap distance is 20 mm in the welding test. The specimens need to be processed before the test is conducted to reduce the influence of the specimen surface on the test results.

Table 2 Parameters of the welding test

Welding current (*I*/A)	Welding time (*t*/Cycle)	Welding pressure (*F*/N)
8800	8	2250
5000	8	2250
5300	8	2250
5600	8	2250
5900	8	2250
6200	8	2250
8800	5	2250
8800	6	2250
8800	7	2250
5000	7	2250
5500	6	2250
6000	5	2250
8800	8	1300
10,000	8	2250
12,000	8	1300

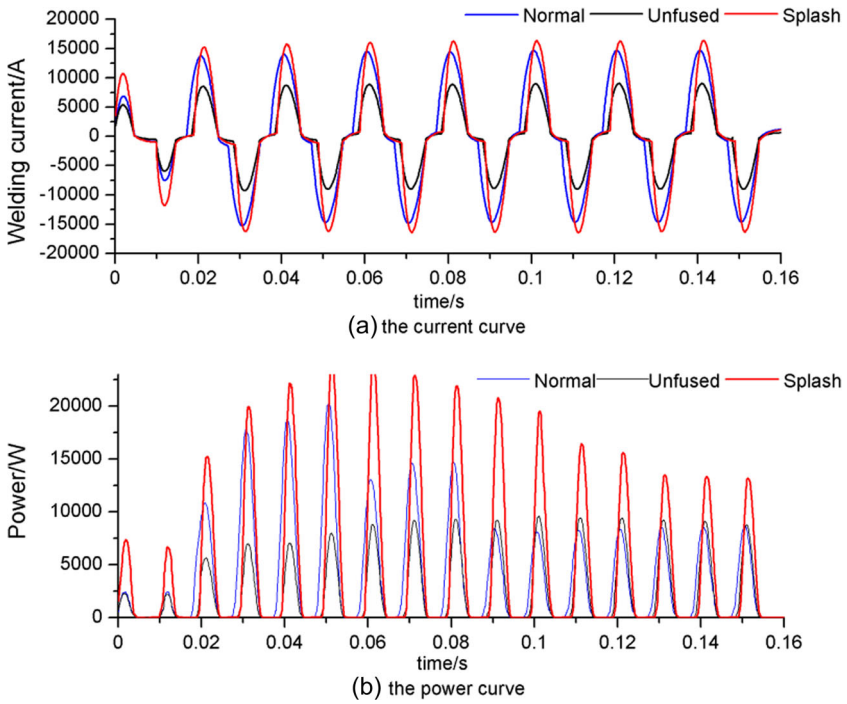

Fig. 2 Current and heat curves under different parameters

The standard welding parameters for 1-mm steel from the Resistance Welding Manufacturing Alliance(RWMA) are shown in Table 1, the specimens need to be processed before the test is conducted to reduce the influence of the specimen surface on the test results, and considering the more accurate relationship between the welding parameters and joint quality, the welding parameters for the test are shown in Table 2. The welding current was in the range of 5000 to 12,000 A, the welding time ranged from 5 to 8 Cycles (1 Cycle = 0.02 s), and the welding pressure ranged between 1300 and 2550 N.

3.3 Tensile test

There are two common indexes to evaluate the joint quality. One is the nugget size and the other is the shear strength. We adopt the second index, which can reflect the state of the joint to a certain extent. For example, when the joint is unfused, the shear strength is smaller than normal.

The device used in the tensile test is the electro-hydraulic servo fatigue testing machine (EHF-EV101K1-030-1A, Japan) produced by SHIMADZU. To obtain the shear strength, it is necessary to test the specimens welded in the welding test.

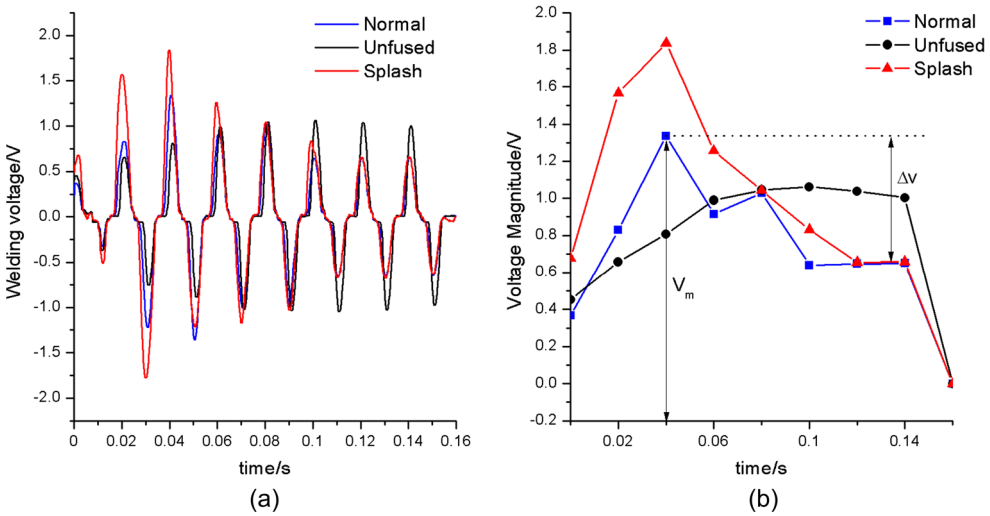

Fig. 3 Comparison of the voltage curves in the normal state and the splash state

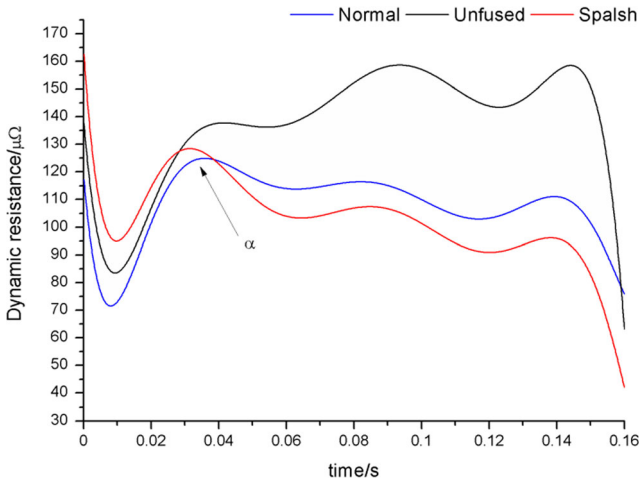

Fig. 4 The dynamic resistance curves

4 Feature extraction

4.1 Welding current

The basic principle of the RSW is that, under the effect of pressure, the joule heat generated by the welding current on the welding zone forms the joint. Therefore, the important factors influencing the joint quality are the welding current, dynamic resistance, and welding pressure.

$$Q = \int_{t_1}^{t_2} I^2(t)R(t)dt \tag{9}$$

where Q is joule heat, $I(t)$ is the welding current, $R(t)$ is the dynamic resistance, and t is the welding time. When the welding time and resistance are constant, the joule heat generated under the welding current is directly proportional to the square of the current. The current, whose influence on the joint shear strength is greater than either that of the welding time and the resistance, is the main influencing factor generating the heat. Meanwhile, it is demonstrated that the current can characterize the welding power in the welding process.

Due to the constant current pattern employed in the RSW machine, the current effective value shown in Fig. 2a can keep constant in the welding process. The following welding parameters are shown in Fig. 2: Normal I = 8800 A, t = 8 Cycle, and F = 2250 N; Unfused I = 5000 A, t = 8 Cycle, and F = 2250 N; and Splash I = 12000 A, t = 8 Cycle, and F = 1300 N. The welding power curves (Fig. 2b) can reflect the different joint states in the RSW and change with the current. Thus, the power (P) and the effective value of the welding current ($I_{\bar{x}}$) are selected as features.

4.2 Welding voltage

As shown in Fig. 3, due to the variation of the welding zone conductivity and the loop impedance, the voltage changes based on certain rules in the welding process. For a normal operation (I = 8800 A, t = 8 Cycle, F = 2250 N), the conductivity rapidly increases with the temperature at the initial welding period, causing the associated voltage to also increase. With an increase in temperature, the rate of conductivity increase diminishes and the contact area increases, which causes the voltage to gradually increase and reach a peak, V_m. As the temperature increases further, the voltage decreases and arrives at a steady state, whose value decreases Δv compared

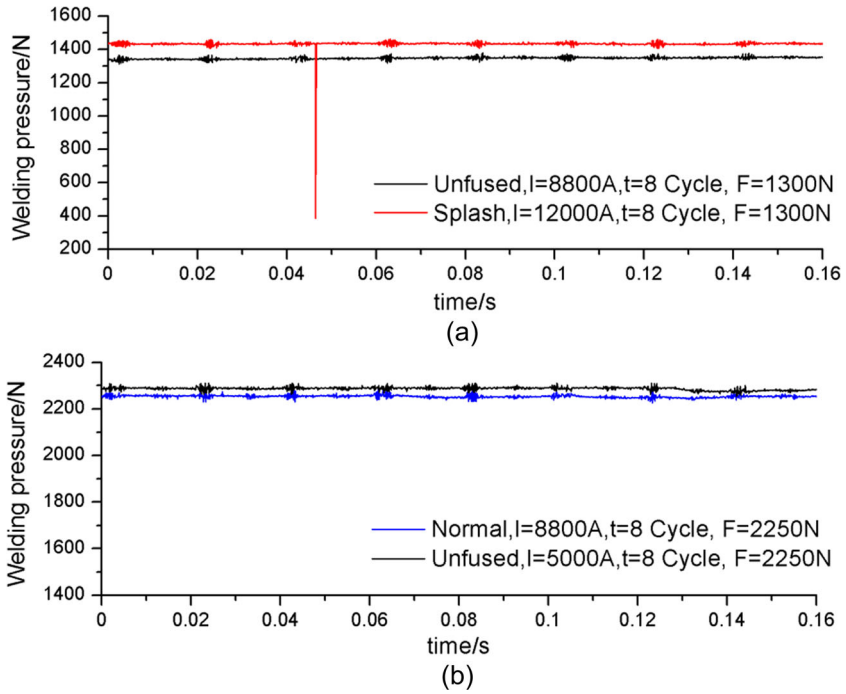

Fig. 5 The comparison of the pressure curves under different parameters

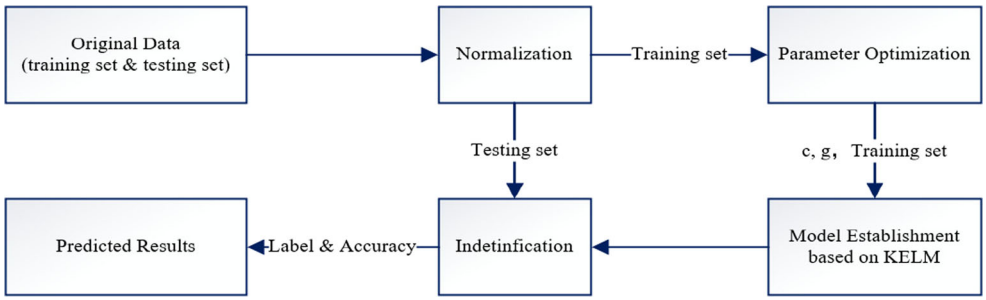

Fig. 6 The process of quality identification

with the peak, V_m. For the splash operation (I = 12,000 A, t = 8 Cycle, F = 1300 N), the higher current leads to a faster increased speed in the initial period and a sharp decline. However, due to an insufficient current (I = 5000 A, t = 8 Cycle, F = 2250 N) forming a joint, it takes more time to arrive at steady state conditions, and the nugget size is smaller on the unfused occasion. Therefore, Δv and $\Delta v/V_m$ are selected as the features.

4.3 Dynamic resistance

Dynamic resistance is the resistance of the current loop that often reflects the dynamic changes in the welding process. The value of the dynamic resistance is obtained by dividing the value of the welding voltage by the current. The variation behaviour between the voltage and the dynamic resistance is generally consistent. Due to different currents, the normal dynamic resistance curve (I = 8800 A, t = 8 Cycle, F = 2250 N) gradually declines after reaching the peak, α, while the splash (I = 12,000 A, t = 8 Cycle, F = 1300 N) sharply declines while the unfused (I = 5000 A, t = 8 Cycle, F = 2250 N) is still increasing (Fig. 4). Therefore, the resistance mean value (R_m) after reaching peak, α, can characterize the joint state and R_m can be a feature.

4.4 Welding pressure

The welding pressure is one of the most basic RSW conditions. The RSW depends on the welding pressure for compressing artefacts, which is crucial to forming a nugget. The welding current is large enough to cause excessive current density, promote the expansion acceleration of the weld zone metal, and force the melted metal out of the control of pressure, which induces the splash (Fig. 5). In addition, when the splash occurs, the pressure curve exists as a sharp decline. The pressure feature can distinguish the different joint states. Hence, the mean value (F_m) and the mean-squared error (F_{mse}) of the pressure are selected as the features of the joint.

5 Quality identification in RSW

5.1 Establishment of the quality identification model

Figure 6 shows the overall process of quality identification and contains five steps. Step 1: The original data that consists of the attribute values and labels input. As shown in Table 3, the attributes are the welding features described in the previous section and the classification label that represents the joint

Table 3 Description of the original data set

	Symbol	Description
Label	JS	The state of the joint. 1 Normal, 2 Unfused, 3 Splash
Attribute	P	The welding power
	$I_{\bar{x}}$	The effective value of the welding current
	Δv	The declining value compared to the peak shown in Fig. 3.
	$\Delta v/V_m$	The ratio between the peak and the steady state shown in Fig. 3.
	R_m	The mean value of the dynamic resistance after reaching the peak
	F_m	The mean value of the welding pressure
	F_{mse}	The mean-squared error of the welding pressure

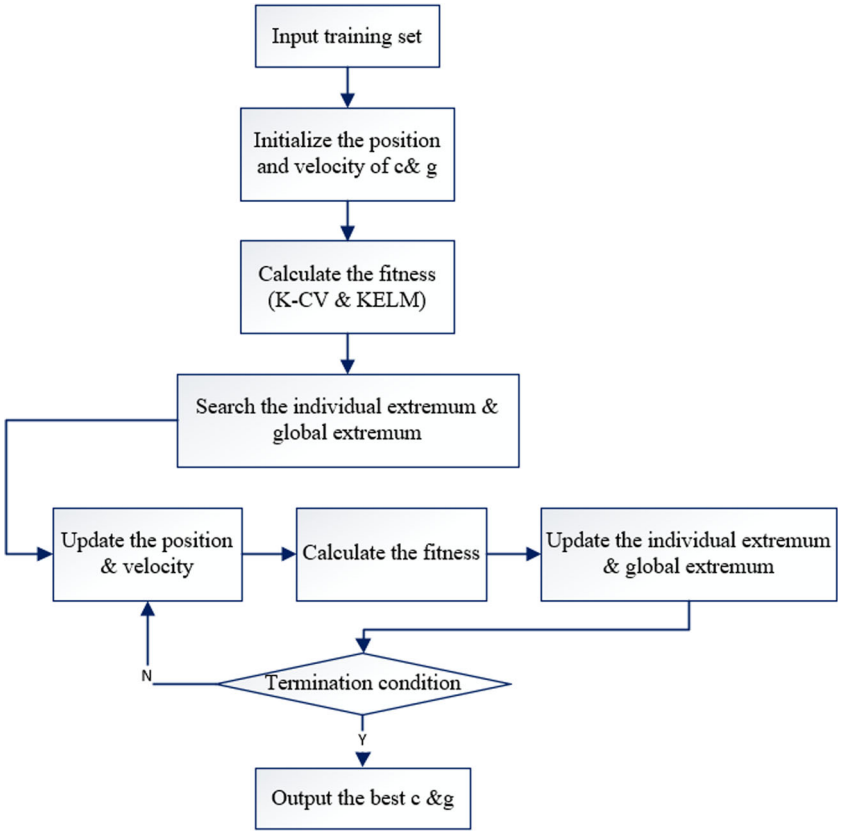

Fig. 7 The process of parameter optimization

Table 4 The welding information of the training set

Welding current (*I*/A)	Time (*t*/Cycle)	Pressure (*F*/N)	Shear strength (*Fs*/N)	Label
8800	8	2250	5861	1
5600	8	2250	5670	1
5900	8	2250	5692	1
6200	8	2250	6039	1
8800	5	2250	5652	1
8800	6	2250	5788	1
8800	7	2250	6041	1
10,000	8	2250	6071	1
10,000	8	2250	5809	1
5000	8	2250	5467	2
5300	8	2250	5519	2
5000	7	2250	5399	2
5500	6	2250	5454	2
6000	5	2250	5338	2
8800	8	1300	5530	2
8800	8	1300	5300	2
8800	8	1300	5496	2
12,000	8	1300	6199	3
12,000	8	1300	6247	3
12,000	8	1300	6185	3
12,000	8	1300	6186	3

Table 5 The comparison between the actual and the model results

Welding current *I*/A	Time *t*/Cycle	Pressure *F*/N	Shear strength *Fs*/N	Real state	Predicted label
8800	8	2250	6050	1	1
8800	8	2250	5953	1	1
8800	8	2250	6000	1	1
8800	8	2250	6056	1	1
5600	8	2250	5744	1	2*
5900	8	2250	5698	1	1
6200	8	2250	5811	1	1
8800	5	2250	5748	1	1
8800	5	2250	5616	1	1
8800	5	2250	5677	1	1
8800	6	2250	5722	1	1
8800	7	2250	6009	1	1
8800	7	2250	6041	1	1
8800	7	2250	6048	1	1
10,000	8	2250	5870	1	1
10,000	8	2250	5888	1	1
10,000	8	2250	5906	1	1
10,000	8	2250	6021	1	1
10,000	8	2250	5922	1	1
10,000	8	2250	5836	1	1
10,000	8	2250	5859	1	1
10,000	8	2250	5812	1	1
5000	8	2250	5467	2	2
5300	8	2250	5427	2	2
5000	7	2250	5427	2	2
5000	7	2250	5374	2	2
5000	7	2250	5320	2	2
5500	6	2250	5392	2	2
5500	6	2250	5381	2	2
5500	6	2250	5369	2	2
6000	5	2250	5401	2	2
8800	8	1300	5349	2	2
8800	8	1300	5300	2	2
8800	8	1300	5343	2	2
8800	8	1300	5496	2	2
8800	8	1300	5261	2	2
8800	8	1300	5375	2	2
8800	8	1300	5386	2	2
8800	8	1300	5381	2	2
8800	8	1300	5348	2	2
12,000	8	1300	6257	3	3
12,000	8	1300	6065	3	3
12,000	8	1300	6324	3	3
12,000	8	1300	6148	3	3
12,000	8	1300	6269	3	3
12,000	8	1300	6142	3	3

state (1 Normal, 2 Unfused, 3 Splash). Step 2: It is essential that the attributes are normalized to avoid the influence on the final predicted result caused by the different sizes of the attributes. In this paper, the attributes are scaled into the interval of [−1, 1]. Step 3: In order to optimize the penalty parameter, C, and kernel parameter,g, we adopt the PSO and K-fold cross validation, which is a useful approach for an unbiased evaluation of the classification (as shown in Fig. 7). This study sets K to 5 and the data are divided into five subsets. In each iteration, one of the five subsets is used as the test set and the remaining four subsets form the training set. Then, the average of the five trials is obtained to improve the reliability of the result. Step 4: Use the training set and the optimal parameters to model the joint quality identification. Step 5: Utilize the model to classify the testing set, and finally obtain the predicted label and accuracy of the test samples.

5.2 Comparison experiment

Information regarding 21 selected samples that form the welding test is presented in Table 4 and the training set of the RSW quality identification model is selected. The optimal parameters $c = 0.1$ and $g = 0.01$. Then, the RSW quality identification model is built. To evaluate the accuracy and reliability of the proposed model, the welding test and the shear test are conducted to obtain the testing set and the real state of joint.

In Table 5, the asterisk denotes that the model-predicted label is not consistent with the real state of the joint. Thus, there is only one predicted label that differs from the real state of joint. The table shows that for the 46 samples, the proposed model has an accuracy of 97.83%. It can be concluded that the RSW quality identification model has a good generalization performance.

6 Conclusion

In this study, feature extraction combined with an analysis of the welding signals is effective and reasonable, which increases the understanding of the welding process. A method for the RSW quality identification based on the PSO and KELM is proposed, which enables the identification of three stages in the RSW quality that include the normal, unfused, and splash. It is demonstrated that the proposed model has a good generalization performance with an accuracy of 97.83% in the comparison test.

Acknowledgments This work was supported by the National Natural Science Foundation of China (Grant No.51335003).

References

1. Gedeon SA, Sorensen CD, Ulrich KT, Eagar TW (1987) Measurement of dynamic electrical and mechanical properties of resistance spot welds. Weld J 66(12):378–385
2. Luo Y, Liu J, Xu H, Xiong C, Liu L (2009) Regression modeling and process analysis of resistance spot welding on galvanized steel sheet. Mater Des 30(7):2547–2555
3. Wan X, Wang Y, Zhao D (2016) Multi-response optimization in small scale resistance spot welding of titanium alloy by principal component analysis and genetic algorithm. Int J Adv Manuf Technol 83(1–4):545–559
4. Satpathy MP, Moharana BR, Dewangan S, Sahoo SK (2015) Modeling and optimization of ultrasonic metal welding on dissimilar sheets using fuzzy based genetic algorithm approach. Engineering Science and Technology, an International Journal 18(4):634–647
5. Yu J (2015) Quality estimation of resistance spot weld based on logistic regression analysis of welding power signal. Int J Precis Eng Manuf 16(13):2655–2663
6. Wan X, Wang Y, Zhao D (2016) Quality monitoring based on dynamic resistance and principal component analysis in small scale resistance spot welding process. The International Journal of Advanced Manufacturing Technology:1–9
7. Zhao D, Wang Y, Lin Z, Sheng S (2013) An effective quality assessment method for small scale resistance spot welding based on process parameters. NDT & E International 55:36–41
8. Ling S-F, Wan L-X, Wong Y-R, Li D-N (2010) Input electrical impedance as quality monitoring signature for characterizing resistance spot welding. Ndt & E International 43(3):200–205
9. Wan X, Wang Y, Zhao D (2016) Multiple quality characteristics prediction and parameter optimization in small-scale resistance spot welding. Arab J Sci Eng 41(5):2011–2021
10. Zhang H, Wang F, Xi T, Zhao J, Wang L, Gao W (2015) A novel quality evaluation method for resistance spot welding based on the electrode displacement signal and the Chernoff faces technique. Mech Syst Signal Process 62:431–443
11. Zhang H, Hou Y, Zhang J, Qi X, Wang F (2015) A new method for nondestructive quality evaluation of the resistance spot welding based on the radar chart method and the decision tree classifier. Int J Adv Manuf Technol 78(5–8):841–851
12. Huang G-B, Zhu Q-Y, Siew C-K (2006) Extreme learning machine: theory and applications. Neurocomputing 70(1):489–501
13. Zong W, Huang G-B (2011) Face recognition based on extreme learning machine. Neurocomputing 74(16):2541–2551
14. Kennedy J (2011) Particle swarm optimization. In: Encyclopedia of machine learning. Springer, pp 760–766
15. Liu J (2009) The research of basic theory and improvement on particle swarm optimization. Central South University
16. Huang G-B, Ding X, Zhou H (2010) Optimization method based extreme learning machine for classification. Neurocomputing 74(1):155–163
17. Huang G-B, Zhou H, Ding X, Zhang R (2012) Extreme learning machine for regression and multiclass classification. IEEE Transactions on Systems, Man, and Cybernetics, Part B (Cybernetics) 42(2):513–529